

R²Human: Real-Time 3D Human Appearance Rendering from a Single Image

Qiao Feng^{1,†}, Yuanwang Yang^{1,†}, Yu-Kun Lai², Kun Li^{1,*}
¹Tianjin University, China ²Cardiff University, United Kingdom

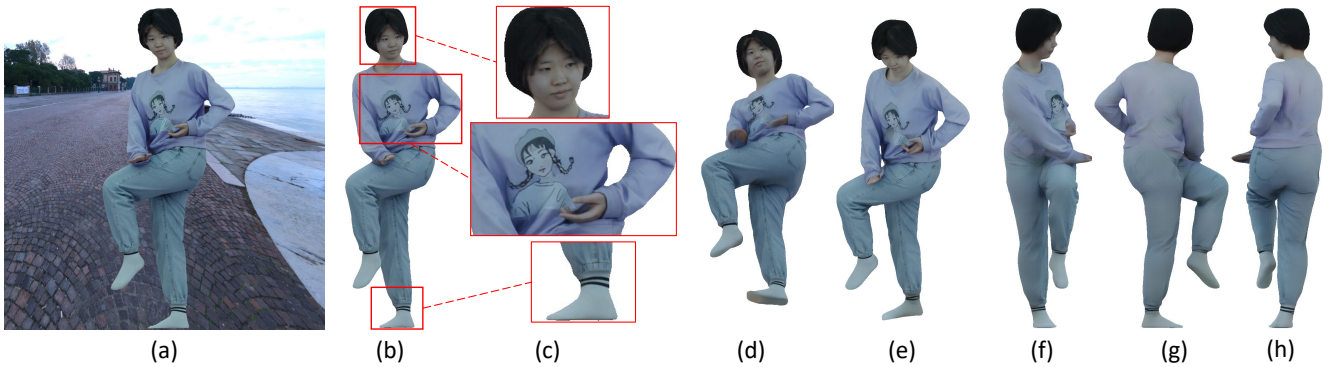


Figure 1. Given a single RGB image, R²Human can generate photorealistic 3D human appearance in real-time. We utilize the input (a) to render close views (b) and zoomed in (c). The results of pitch angle changes are shown in (d-e), while (f-h) demonstrate the outcomes of divergent views.

Abstract

Reconstructing 3D human appearance from a single image is crucial for achieving holographic communication and immersive social experiences. However, this remains a challenge for existing methods, which typically rely on multi-camera setups or are limited to offline operations. In this paper, we propose R²Human, the first approach for real-time inference and rendering of photorealistic 3D human appearance from a single image. The core of our approach is to combine the strengths of implicit texture fields and explicit neural rendering with our novel representation, namely Z-map. Based on this, we present an end-to-end network that performs high-fidelity color reconstruction of visible areas and provides reliable color inference for occluded regions. To further enhance the 3D perception ability of our network, we leverage the Fourier occupancy field to reconstruct a detailed 3D geometry, which serves as a prior for the texture field generation and provides a sampling surface in the rendering stage. Experiments show that our end-to-end method achieves state-of-the-art performance on both synthetic data and challenging real-world images and even outperforms many offline meth-

ods. The project page is available for research purposes at <http://cic.tju.edu.cn/faculty/likun/projects/R2Human>.

1. Introduction

The rapid evolution of digital technology has notably impacted computer graphics and computer vision, particularly in 3D human appearance reconstruction. This advancement not only enhances visual experiences but also paves the way for practical applications in AR/VR, enabling interactive platforms like holographic communication and immersive social experiences. However, existing methods heavily rely on multi-camera setups [15, 19, 20, 31] or are constrained to offline operations [1, 7, 16], leaving real-time 3D human rendering from a single image as an unresolved challenge. In this paper, we aim to render the photorealistic 3D human appearance in real-time from a single image, as shown in Fig. 1.

Research in human novel view synthesis has explored various methodologies, which can be roughly classified into two categories. The first category of methods [2, 19, 31] is founded on flow-based neural rendering, which warps the feature map from the input images to the target view and then produces high-quality novel view results with convo-

† Equal contribution.

* Corresponding author.

lutional neural networks (CNNs). However, the network’s predictions for occluded regions in the input image usually exhibit significant randomness due to the lack of 3D structure understanding, making it challenging to obtain consistently accurate results. To deal with this, these methods require multi-view input images to cover the rendering area as comprehensively as possible. Consequently, generating photorealistic renderings from only one image becomes difficult for them.

Another category of methods aims to recover a 3D consistent appearance for the human body. PIFu [16] recovers the 3D human geometry and appearance from a single human image using an occupancy field and a texture field, respectively. However, the rendered images are of low quality and the process is time-consuming. Its follow-up work [1] disentangles lighting from texture and redesigns the loss functions, resulting in improved visual quality. On the other hand, works utilizing the Neural Radiance Fields (NeRF) [7, 13, 15, 20] predict the density and radiance throughout the 3D space for rendering images by integrating along camera rays. However, NeRF-based methods often struggle with single-view inputs. While approaches above vary in human appearance representations, they share a common paradigm: they estimate geometry and color for discrete sampled points independently. This makes it difficult for the models to discern relationships between the sampled points, resulting in relatively lower quality in the synthesized novel view images. Additionally, these methods require dense spatial sampling, which results in high computational costs and makes it challenging to balance real-time performance with rendering quality.

In this paper, we introduce R^2Human , a real-time framework for rendering human appearance, which uniquely combines flow-based rendering techniques with an implicit 3D human geometry representation to synthesize novel view images. Our method only requires a single image as input and achieves both high-quality and real-time rendering performance. Moreover, our method can generate novel view renderings of humans in various clothing without individual-specific training. Unlike previous flow-based rendering methods that omit points occluded in the source view, we introduce an intermediate representation, namely the Z-map, during the rendering process, which collects the source view depth of the rendered points of the target view and forms them to a 2D map. It helps lift the 2D image feature into a 3D texture feature field, while maintaining compatibility with 2D neural rendering networks. This unique capability enables our network to learn data-driven 2D appearance knowledge of clothed human images, resulting in more accurate renderings. By preserving the features of occluded points and leveraging the Z-map, our method effectively resolves depth ambiguities. Additionally, we employ an efficient 3D object representation known as Fourier oc-

cupancy fields (FOF) [4], which explicitly represents a 3D object as a multi-channel image. It can serve both as a prior for texture field generation and as a sampling surface during the rendering stage, avoiding the high computational costs caused by dense sampling. Our method paves the way for the practical applications of AR/VR, which can be applied in holographic communication in the future.

In summary, the contributions of our work are as follows:

- We present a novel system for high-quality, real-time synthesis of human novel view images with only a single RGB image input. To the best of our knowledge, this is the first system to restore the full-body appearance of a 3D human in real-time from a single image.
- We propose R^2Human , an end-to-end CNN-based neural rendering method that combines the strengths of implicit texture field and explicit neural rendering, which can produce results with both 3D consistency and high visual quality.
- We introduce an intermediate representation called Z-map, which alleviates depth ambiguities in rendering, enabling high-fidelity color reconstruction for the visible area while providing reliable color inference for the occluded regions.

2. Related work

2.1. Monocular 3D Human Reconstruction

Human reconstruction has long been a concern in the domain of computer vision and graphics. Methods for predicting human bodies from a single image represent 3D shapes primarily by estimating the properties of points in 3D space. Some previous works [21, 29] directly predict the occupancy field of a given segment in space through regression networks, but such methods have high memory requirements, which limits the spatial resolution of shape estimation. Another type of methods involves using implicit function networks to remove resolution constraints. Saito *et al.* [16] proposed an implicit function based on pixel-aligned features to reconstruct a 3D human from a single image. PIFuHD [17] further introduces normal maps to improve geometric details. Subsequent methods [24, 25, 30] improve the robustness of the results by incorporating parametric SMPL [12] priors. Although these methods can achieve realistic results, they often require significant computational resources and are time-consuming. Feng *et al.* [4] proposed an efficient 3D geometric representation called Fourier Occupancy Field, which can represent a high-quality 3D geometry as a multi-channel image. It establishes a strong link between 3D geometry and 2D images, significantly reducing the computational requirements for reconstruction. However, one limitation is its inability to estimate texture during the geometry reconstruction process.

2.2. Human Novel View Synthesis

Flow-based neural rendering methods can synthesize realistic novel human view images. Shao *et al.* [19] estimate robust appearance flow with epipolar constraints, reduce ambiguous texture warping, and then synthesize high-quality novel human perspective. Zhou *et al.* [31] first estimate highly detailed 3D human geometry, and then effectively solve the serious occlusion problem caused by sparse views through geometry-guided pixel-wise feature integration method. Although these methods reduce the impact of occlusion on flow-based texture warping, they still require multi-view information to ensure the robustness of the results. Phong *et al.* [14] warp images from a single sparse RGB-D input by sphere-based rendering and refine the resulting image using an additional occlusion-free input, but its application is limited by its reliance on depth sensors. On the other hand, some methods [16, 25, 26] that focus on geometry can predict textures during reconstruction, and then synthesize novel views through traditional rendering methods. Thiemo *et al.* [1] improved the visual fidelity of the results by computing albedo and shading information and carefully designing rendering losses. However, these methods find it difficult to learn the relationships between points in space due to the use of discrete sampling points to estimate color, resulting in relatively poor rendered image quality.

In recent years, neural radiance fields (NeRF) [13] have become a powerful novel view synthesis tool, using multi-layer perceptrons (MLP) to model a scene as density and color fields, resulting in realistic rendering. Researchers have made many attempts on the basis of NeRF. Peng *et al.* [15] anchor the learned potential encoding onto SMPL [12] fixed points to integrate multi-view video information, but it can only render humans with relatively uniform textures. Shao *et al.* [20] combine the surface field and the radiance field to achieve high-quality rendering, but are still limited by the need for multiple views. Hu *et al.* [7] proposed the first generalizable Human NeRF based on a single image input, but visible artifacts still exist in partially occluded bodies in the observation space. In addition, these implicit representation based methods all have a common problem: due to the high computational complexity required for dense sampling, they are time-consuming.

In this paper, we contribute the first real-time and high-quality human novel view synthesis system from a single RGB image, which combines the strengths of implicit texture field and explicit neural rendering, opening up novel possibilities for holographic communication and immersive social interaction. Tab. 1 presents a comparative analysis focusing on key features: support for monocular input, real-time processing capabilities, full-body rendering, and high-fidelity novel view synthesis. As indicated in the table, our method is unique in its support for all these features, distin-

guishing it from other approaches.

Table 1. Comparison with state-of-the-art methods. Novel view synthesis mean high-fidelity results. ✗: not supported, ✓: supported.

Method	Monocular Input	Real-time Processing	Fully-body Rendering	Novel View Synthesis
Project Starline [10]	✗	✓	✗	✓
3DTexture [22]	✗	✗	✓	✗
Floren [19]	✗	✗	✓	✓
HDHuman [31]	✗	✗	✓	✓
PIFu [16]	✓	✗	✓	✗
SHERF [7]	✓	✗	✓	✗
Ours	✓	✓	✓	✓

3. Preliminary

FOF [4] introduces a novel, powerful, efficient and flexible 3D geometry representation called Fourier occupancy field, for real-time and accurate human reconstruction from a single image. The Fourier Occupancy Field represents a 3D object with a 2D field orthogonal to the view direction. Specifically, FOF approximates the 1D occupancy signal of point (x, y) on the 2D plane orthogonal to the direction of the view with a subspace spanned by the first $2N + 1$ basis functions of a convergent Fourier series:

$$f(z) = \frac{a_0}{2} + \sum_{n=1}^{2N+1} (a_n \cos(nz\pi) + b_n \sin(nz\pi)), \quad (1)$$

where $\{a_n\}, \{b_n\} \in \mathbb{R}$ are coefficients of basis functions $\{\cos(nx)\}$ and $\{\sin(nx)\}$, respectively. Then, the human geometry is represented as

$$F(x, y, z) = b^T(z)C(x, y), \quad (2)$$

where $b^T(z)$ is the vector of the first $2N + 1$ basis functions spanning the approximation subspace, and $C(x, y)$ is the $2N + 1$ Fourier coefficient vectors for the 1D occupancy signal at (x, y) . FOF stores a 3D object as a multi-channel image that can be quickly restored to a 3D occupied field by matrix multiplication, which facilitates prediction using a CNN.

4. Method

Our goal is to build an end-to-end trainable framework that can achieve photorealistic novel view rendering of humans from a single RGB image. We employ FOF [4] to represent the 3D human form as a multi-channel image, thereby reducing computational time and memory overhead. Additionally, we introduce Z-map to effectively address the issue of prediction ambiguity for occluded points within the input image. Consequently, our network is capable of producing high-quality renderings of novel views using just a

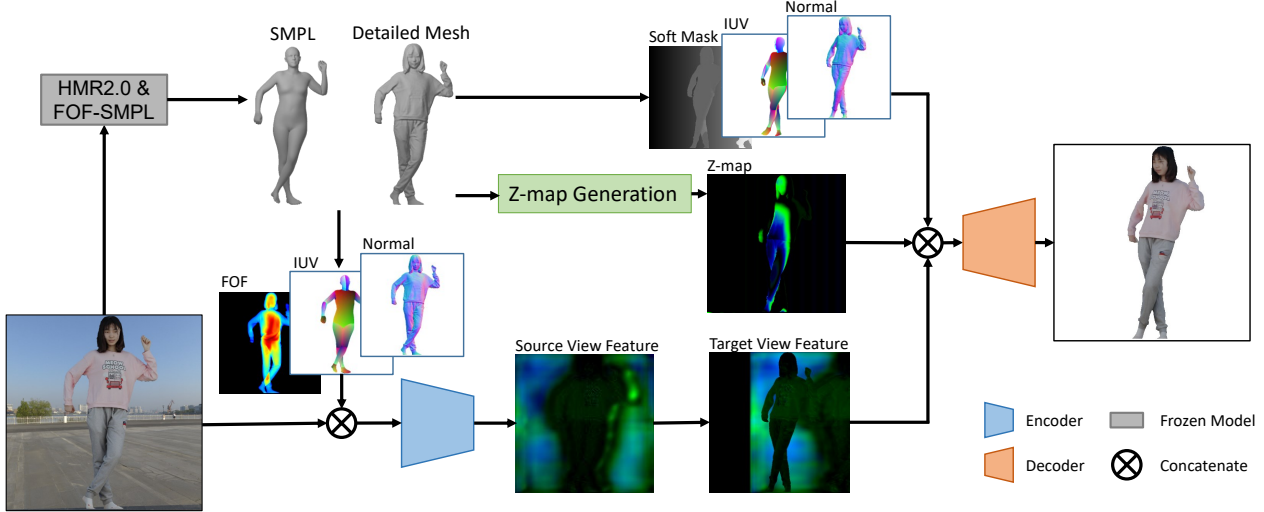


Figure 2. **Overview of R^2 Human**: To render the target image, we first estimate the SMPL model and a detailed mesh from the input image with HMR2.0 and FOF-SMPL. Then, the input image, together with the FOF representation and other rendered priors, are encoded into a feature map. The feature is transformed to the target view, combined with Z-map, soft mask, target IUUV, and target normal map, and decoded to the final result through the CNN renderer.

single image. As shown in Fig. 2, our framework mainly consists of three parts: 1) We use a reconstruction network to generate a Fourier occupation field from a single image. 2) We develop an image encoder to generate a texture field aligned with the reconstructed 3D geometry. 3) Finally, we warp the texture field and obtain other priors, and then use a rendering network to synthesize results with high visual quality.

4.1. Z-map

Most existing methods taking a single image as input rely on a pixel-aligned implicit function to produce a 3D field, such as a texture field. The color of a point in 3D space can be predicted by:

$$c = f_{mlp}(e, z), \quad (3)$$

where $c \in \mathbb{R}^3$ is the predicted RGB color, e is the corresponding feature sampled from the image feature map, z is the source view depth of that point, and f_{mlp} is the MLP-based decoder. In the task of view synthesis, each pixel on the output image I corresponds to a point in the 3D space. Thus, we can collect the colors c for all those points to generate the final result.

Such a schema does not consider the internal relationship between those points. In contrast, flow-based methods decode those features simultaneously to avoid such a drawback, which can be written as:

$$I = f_{cnn}(F_{map}(\mathcal{F}_s)), \quad (4)$$

where \mathcal{F}_s is the feature map of the source view, F_{map} is the wrapping flow, and f_{cnn} is the CNN-based decoder.

Let $\mathcal{F}_t = F_{map}(\mathcal{F}_s)$ be the feature map corresponding to the target view. We can notice that \mathcal{F}_t is the collection of e in Eq. 3. Therefore, if we collect all those source view depth values and form them into a 2D Z-map, these two kinds of methods can be unified in a single framework:

$$I = f_{cnn}(\mathcal{F}_t, Z_{map}), \quad (5)$$

where Z_{map} is the Z-map. Like the warping flow, Z-map can also be directly produced, which is more efficient than calculating z values for each point separately.

As illustrated in Fig. 3, the Z-map establishes a depth correspondence between the source and novel views. It aligns with the novel view; however, each pixel in the Z-map represents the depth of its corresponding point in the source view. Utilizing the source view’s depth information enables the decoder to more effectively leverage features from the input image. Additionally, the depth value in Z-map makes it possible to produce different colors for a specific image feature vector, which helps the network to perform more reasonable inference for invisible points.

4.1.1 Calculation of Z-map

To combine the strengths of implicit texture field and explicit neural rendering, we propose the Z-map, which enables rendering networks to achieve 3D perception and avoid one-to-many problems caused by depth ambiguity. We define Z-map as the depth obtained from the transformation of visible points in the novel view to the source view, so we can obtain Z-map while calculating the flow maps. Specifically, we render the depth maps D_s, D_t first for both views using the predicted mesh based on camera

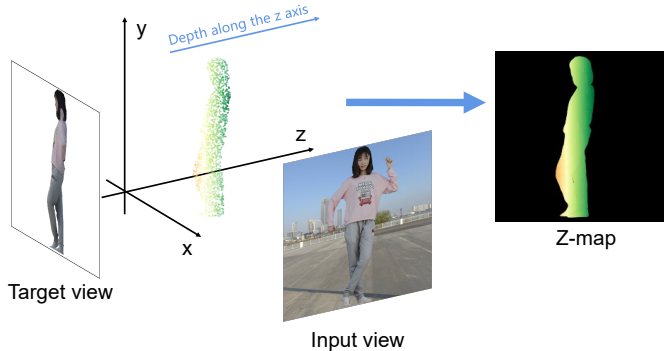


Figure 3. Z-map visualization example.

parameters. Then, for each coordinate point $v_t \in \mathbb{R}^2$ in the novel view, we inverse project it to the world coordinate system using the camera parameters, and then project it to the source view space to obtain flow maps and Z-map from the novel view to the source view:

$$(F_{map}, Z_{map}) = \Pi^s((\Pi^t)^{-1}(v_t, D_t)), \quad (6)$$

where Π^s is the projection matrix transforming points from the world coordinates to the source view coordinates v_s and $(\Pi^t)^{-1}$ is the matrix transforming points from the novel view coordinates v_t to the world coordinates.

4.2. R²Human Networks

4.2.1 Pixel-aligned Feature Encoder.

To leverage the geometric information obtained from the reconstruction network and enhance feature extraction, our encoder incorporates additional information derived from the reconstructed geometry. This allows for a more comprehensive understanding of the input image. This approach consists of three key components: FOF, normal map, and IUV map.

FOF. As shown in Fig. 2, we obtain FOF through the existing method. It is a multi-channel image that contains 3D information and enables the encoder to capture and represent spatial relationships, depth cues, and other geometric aspects inherent in the Human. This can lead to a more robust and information-rich representation of features, potentially improving the performance of subsequent rendering.

Normal map. We generate a normal map by calculating the surface normals for each point in the predicted mesh. It can enhance the encoder’s ability to perceive lighting information and geometric details.

IUV map. we add an auxiliary pixel-level dense correspondence as a prior knowledge to improve the reliability of network extraction because of the regularity of human textures. Specifically, we use the IUV map defined in DensePose [5] as the dense correspondence representation, which includes

the partitioning and UV parametrization of the mesh surface.

In summary, our encoder network E is defined as follows:

$$\mathcal{F}_s = E(\oplus(I_s, C_s, N_s, A_s)), \quad (7)$$

where \oplus is the concatenation operation. I_s, C_s, N_s, A_s are the input color images, the predicted FOF, estimated surface normal and IUV maps, respectively. Note that our IUV map is rendered based on SMPL models [12] estimated from the input images.

4.2.2 Novel View Rendering.

Similar to the encoder, our rendering network also integrates some additional information to improve rendering performance. Note that we do not integrate Fourier occupation fields because rendering only focuses on the visible part of the image. We use novel camera parameters Π^t to render the normal map and IUV map, respectively. In addition to using the Z-map mentioned in Sec. 4.1, we also calculate soft masks as conditions to enable the network to understand the occlusion relationships between different views. We define the soft mask as the difference between the depth of the source image D_s and the depth projection of the novel view onto the source view:

$$M(v_t) = \Pi^s((\Pi^t)^{-1}(v_t, D_t)) - D_s(v_t), \quad (8)$$

Then we warp the features of the source view to the novel view based on the flow map:

$$\mathcal{F}_t(v) = \mathcal{F}_s(F_{map}(v)), \quad (9)$$

In summary, our rendering network R is defined as follows:

$$I_t = R(\oplus(\mathcal{F}_t, Z_{map}, M, N_t, A_t)), \quad (10)$$

where N_t, A_t are the normal map and IUV map rendered by novel camera Π^t , respectively.

4.3. Loss Function

The loss functions used have a significant impact on the details recovered by the final model. For our rendering network, the output is a high-resolution image I_{512} rendered from the target camera Π^t . We used the weighted sum for multiple loss terms as follows:

$$L = \lambda_1 L_{pixel} + \lambda_2 L_{LPIS} \quad (11)$$

where L_{pixel} is the common L_1 loss for direct supervised pixel points between I_{512} and ground truth \hat{I}_{512} ; L_{LPIS} is the LPIPS perceptual loss [28] computed over pairs (I_{512}, \hat{I}_{512}) ; λ_1 is 1 and λ_2 is 0.5 in our experiments. As shown in the figure[], the LPIPS perceptual loss can effectively improve the reconstruction effect of the model on faces when the angle transformation is large.



Figure 4. Novel view rendering on THuman2.0 dataset. The results show that our method is superior to other methods in some challenging human poses. We recommend zooming in to get a better view of the details.

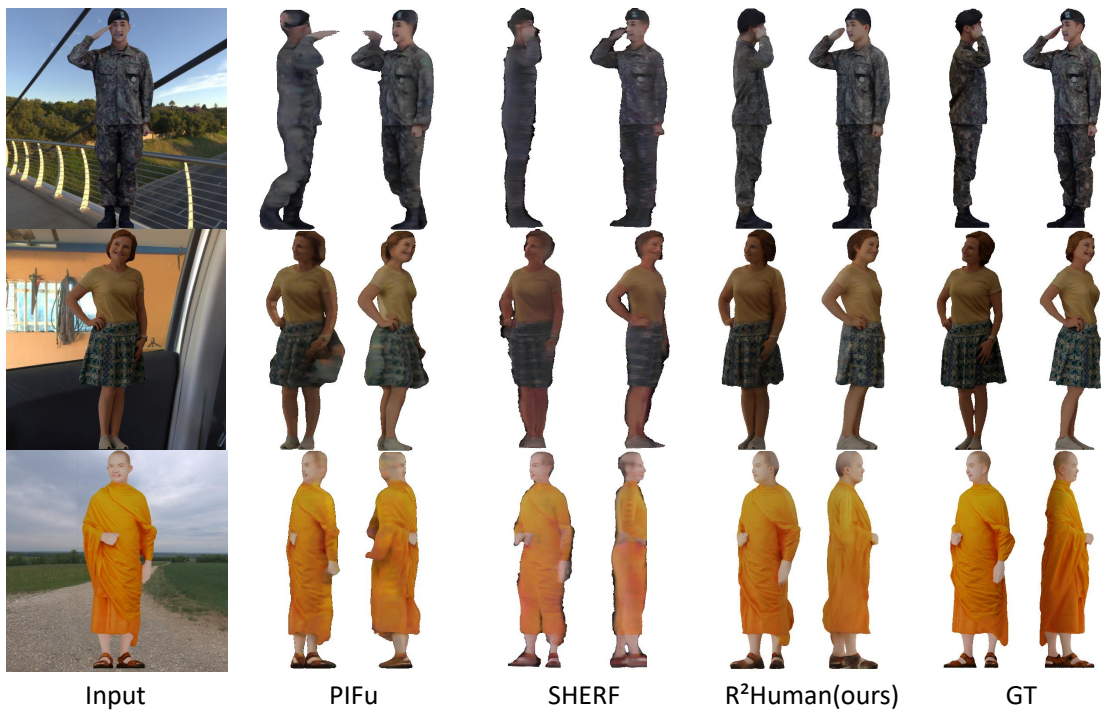


Figure 5. Novel view rendering on 2k2k dataset. The results show that our method can better adapt to different body types and loose clothing. We recommend zooming in to get a better view of the details.

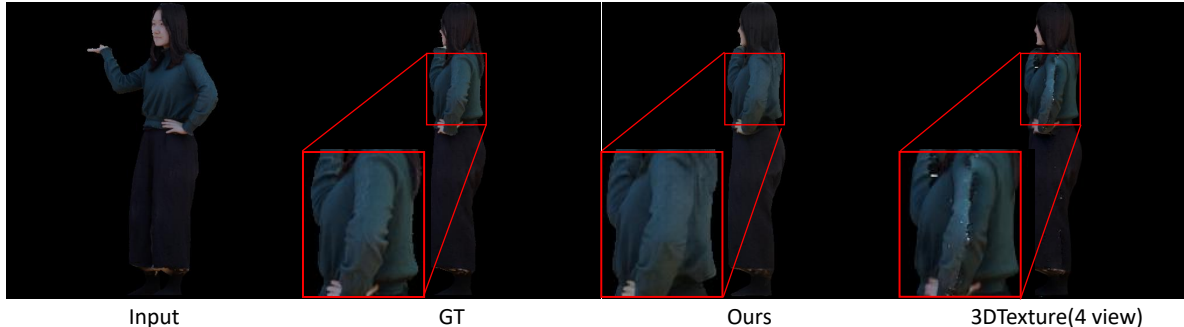


Figure 6. Qualitative comparison with 3DTexture. The results show that even with four views, our single-view approach still outperforms traditional texture mapping.

5. Experiments

5.1. Implement Details

Dataset. Our our network is trained on synthetic data including pairs of meshes and rendered images. We collect 526 high-quality human scans from THuman2.0 dataset [27] with a wide range of clothing, poses and shapes. We randomly split them into a training set of 368 scans and a testing set of 105 scans. The remaining subjects are used as the validation set. For each scan, we render 32 views of high-resolution images with 16 lighting settings randomly selected from 630 lightings.

Training. For training our network, instead of using FOF constructed from the ground truth geometry, we apply the FOF-based reconstruction network [4] to predict the FOF representation from the single-view input image. Using the predicted FOF for training can make the rendering network obtain stronger generalization ability and improved robustness. We implement our method using PyTorch and train all network components jointly, end-to-end, using the Adam optimizer, with a learning-rate of 2×10^{-4} . We train the network for 10 epochs which takes about 4 days with a batch size of 5 using a single NVidia RTX3090 GPU.

5.2. Comparisons

Metrics. We use three widely used metrics for images to quantitatively evaluate our method: structural similarity (SSIM) [23], peak signal-to-noise ratio (PSNR) [18], and learned perceptual image patch similarity (LPIPS) [28] that uses AlexNet [9] to extract features.

Baselines. We quantitatively compare our approach with two methods [7, 16]: 1) PIFu [16] uses implicit functions based on pixel-aligned features to reconstruct 3D humans from a single image, and we use a standard rendering pipeline to render it to obtain a novel view image. 2) SHERF [7] is the first generalizable Human NeRF model to recover 3D humans from a single image, achieving state-of-the-art performance compared with previous generalizable Human NeRF methods. Additionally, to showcase the

necessity of utilizing neural rendering, we conducted qualitative comparisons with state-of-the-art texture mapping methods 3DTexture [22].



Figure 7. Ablation study comparing our model with and without the FOF in the encoder.

Qualitative results. Fig. 4 and Fig. 5 presents qualitative comparisons of our approach to the baseline on the 2k2k dataset [6] and the THuman2.0 dataset [27], respectively. PIFu demonstrates the ability to estimate reasonably accurate colors, but its performance is hindered by limitations in geometric estimation, resulting in suboptimal image quality. On the other hand, while SHERF heavily relies on SMPL priors, it struggles to synthesize satisfactory results for larger body sizes or those wearing loose-fitting clothing. Fig. 6 shows a qualitative comparison with traditional texture mapping methods. 3DTexture has a noticeable concatenation artifacts in the multi-view settings and cannot render occluded areas in the input view. Thanks to Z-map, R²human is able to incorporate geometric priors to enhance the rendering of occluded areas by 3D information. Furthermore, with the aid of neural rendering, R²human can effectively compensate for any inaccuracies in the geometric estimates. As a result, R²human is capable of synthesizing high-fidelity results that exhibit remarkable 3D consistency.

Quantitative evaluations. We selected 105 models in the 2k2k and THuman2.0 test sets for evaluation, respectively. Tab. 2 shows the performance of the method when the novel view is in close proximity to the source view (with a differ-

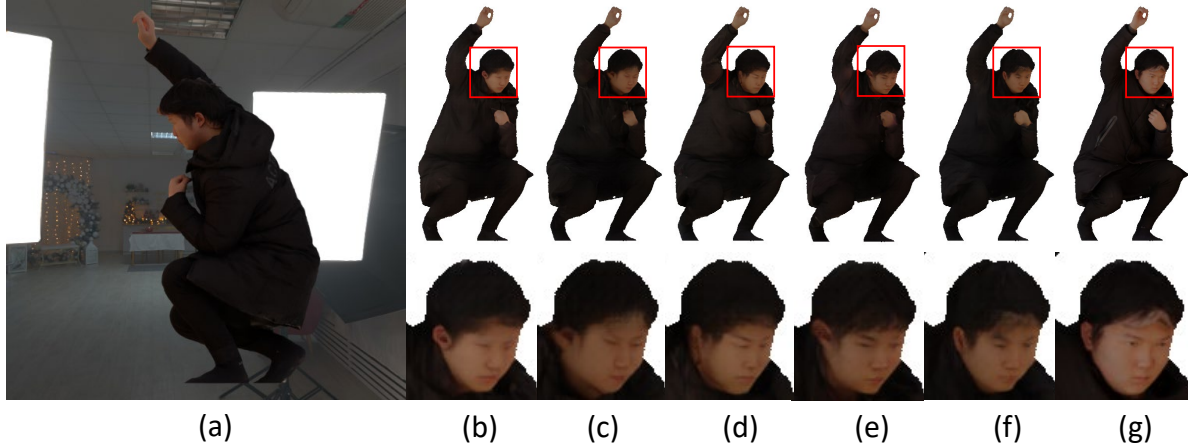


Figure 8. Additional ablation study. (a) The input image, (b) w/o Z-map, (c) w/o normal map, (d) w/o IUUV map, (e) w/o soft mask, (f) full (ours), and (g) ground truth.



Figure 9. Comparison between our model and an ablated model trained without the perceived loss.

ence of $\leq 45^\circ$), and Tab. 3 shows the performance when the novel view is significantly different from the source view (with a difference of $\geq 90^\circ$). It is evident that R²Human outperforms SHERF and PIFu across all evaluation metrics, regardless of whether there are minor or major changes in the viewing angle.

Table 2. Quantitative rendering results in close views.

Method	THuman2.0			2k2k		
	SSIM \uparrow	PSNR \uparrow	LPIPS \downarrow	SSIM \uparrow	PSNR \uparrow	LPIPS \downarrow
PIFu [16]	0.8658	23.33	0.1310	0.8672	23.37	0.1147
SHERF [7]	0.8890	25.50	0.0992	0.8802	24.52	0.1067
Ours	0.9436	29.74	0.0393	0.9214	27.85	0.0527

Table 3. Quantitative rendering results in divergent views.

Method	THuman2.0			2k2k		
	SSIM \uparrow	PSNR \uparrow	LPIPS \downarrow	SSIM \uparrow	PSNR \uparrow	LPIPS \downarrow
PIFu [16]	0.8433	21.90	0.1571	0.8449	21.53	0.1439
SHERF [7]	0.8733	23.85	0.1158	0.8664	22.83	0.1227
Ours	0.9215	28.00	0.0568	0.8902	25.37	0.0796

5.3. Ablation study

We are conducting ablation experiments to compare variants of our architecture and different training strategies.

Effects of Fourier occupation field (FOF) in the encoder.

We remove the FOF input during encoding to verify the effects of 3D information on the results. Quantitative comparisons are in the sixth row of Tab. 4, showing that all three metrics of rendering results without FOF drop. As shown in Fig. 2, FOF can help image encoder better perceive 3D information, thereby reducing rendering artifacts and blurriness.

Table 4. Quantitative evaluation for ablation study on THuman2.0 dataset.

zmap	normal	iuu	mask	SSIM \uparrow	PSNR \uparrow	LPIPS \downarrow
	✓	✓	✓	0.9440	29.57	0.0405
✓		✓	✓	0.9438	29.59	0.0402
✓	✓		✓	0.9433	29.72	0.0395
✓	✓	✓		0.9476	30.18	0.0394
w/o FOF				0.9428	29.50	0.0401
w/o VGG loss				0.9423	29.37	0.0501
Ours(full)				0.9463	30.08	0.0392

Effects of additional information in the rendering network.

Fig. 8 illustrates the comparison of the effects of incorporating additional information into the rendering network. This information is not generated by a neural network but obtained through computer graphics techniques. It is evident that the absence of each representation results in a noticeable decline in visual quality. Tab. 4 presents our quantitative results, with our full approach achieving the highest rank in terms of LPIPS, while ranking second in SSIM and PSNR. This outcome can be attributed to the fact

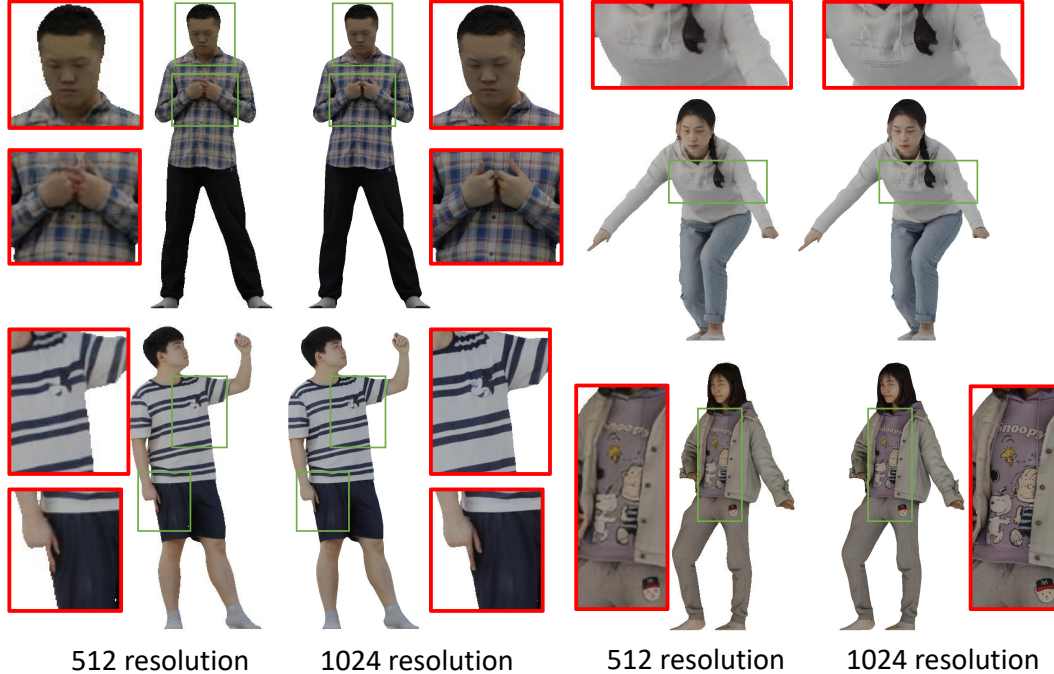


Figure 10. Comparison of results (input view) at low resolution (512×512) and high resolution (1024×1024).

that we do not utilize a ground truth mesh, but instead rely on estimated geometry to compute the mask. As a result, while our visual results appear accurate, there may be some small misalignment in terms of geometric consistency.

Effects of perceptual loss. To explore the effects of perceived loss on training, we retrained a variant without using the perceived loss. Fig. 9 compares results obtained with and without the use of perceived loss, and we also make a quantitative comparison in the seventh line of Tab. 4. The results show that the perceptual loss allows the network to learn more texture details, thus improving the realism of the rendering results.

6. Results on 1K Resolution

Our method is trained and tested on a resolution of 512×512 . We also explore the performance of the method at 1K resolution. Specifically, we have remade a 1K dataset and trained our model on it. Fig. 10 shows the results of our method at high resolution. It can be seen that high-resolution images effectively improve the clarity of the results and enhance the visual effect of the results.

6.1. Application

We apply our method to real-time monocular human novel view synthesis, operates as follows: Images are captured from the video stream using OpenCV [3] and preprocessed to a 512×512 resolution. We then apply RVM [11] for human mask extraction, effectively removing the background,

and use HMR2.0 [8] for SMPL model estimation. Subsequently, the FOF-SMPL [4] is utilized to infer the occupation field. CUDA is employed to accelerate the rendering of depth, normal, and IUUV maps. The final high-fidelity novel view images are rendered in real-time using the rotation matrix R and the previously processed data. Our pipeline, implemented using TensorRT on a single RTX-3090 GPU, achieves a performance of 24+ FPS, with potential for further enhancement via additional GPUs. Fig. 11 and Fig. 12 showcase some of the real-time reconstruction results.

Table 5. time break down.

Component	Streamer	Segmentation & SMPL	FOF-SMPL	Additional information	Inference(Ours)
Time(ms)	4.21	10.59	8.77	0.93	13.13

Tab. 5 details the execution time for each component of our pipeline. Currently, we implement our pipeline serially, achieving an overall runtime of approximately 37ms. We have combined the neural network and tensor multiplication into a single component, optimized using TensorRT for enhanced acceleration. Moreover, there is potential for substantially increasing the pipeline’s processing speed through parallel implementation of each component.

7. Conclusion and Discussion

Conclusion. We propose a novel method, combining the strengths of implicit texture field and explicit neural ren-



Figure 11. Real-time rendering results by our method.



Figure 12. Real-time rendering results by our method.

dering, for real-time inference and rendering of realistic 3D human appearance from a monocular RGB image. Our approach introduces a depth mapping between the novel and source views, which reduces depth ambiguities in rendering and enables high-fidelity color reconstruction. The experimental results show that the proposed method achieves state-of-the-art performance on both synthetic data and real-world environment.

Limitation. Although our method makes full use of the 3D geometry information in the reconstructed data, there may still be artifacts caused by inaccurate geometry estimation when the angle changes are too large. In addition, while our

method can provide relatively consistent results when synthesizing novel views with changing view directions, temporal inconsistencies may still happen because the feature warp varies slightly from frame to frame.

Broader Impact. Our proposed framework has the potential to significantly advance the development of holographic communication. However, high-fidelity novel view synthesis may also raise privacy concerns. Therefore, we strongly recommend that regulators establish ethical guidelines and regulatory frameworks that strike a balance between innovation and privacy protection.

References

- [1] Thiemo Alldieck, Mihai Zanfir, and Cristian Sminchisescu. Photorealistic monocular 3d reconstruction of humans wearing clothing. In *Proceedings of the IEEE/CVF Conference on Computer Vision and Pattern Recognition*, pages 1506–1515, 2022. [1](#), [2](#), [3](#)
- [2] Shai Avidan and Amnon Shashua. Novel view synthesis in tensor space. In *Proceedings of IEEE Computer Society Conference on Computer Vision and Pattern Recognition*, pages 1034–1040. IEEE, 1997. [1](#)
- [3] Gary Bradski. The opencv library. *Dr. Dobb's Journal: Software Tools for the Professional Programmer*, 25(11):120–123, 2000. [9](#)
- [4] Qiao Feng, Yebin Liu, Yu-Kun Lai, Jingyu Yang, and Kun Li. Fof: learning fourier occupancy field for monocular real-time human reconstruction. *Advances in Neural Information Processing Systems*, 35:7397–7409, 2022. [2](#), [3](#), [7](#), [9](#)
- [5] Rıza Alp Güler, Natalia Neverova, and Iasonas Kokkinos. Densepose: Dense human pose estimation in the wild. In *Proceedings of the IEEE conference on computer vision and pattern recognition*, pages 7297–7306, 2018. [5](#)
- [6] Sang-Hun Han, Min-Gyu Park, Ju Hong Yoon, Ju-Mi Kang, Young-Jae Park, and Hae-Gon Jeon. High-fidelity 3d human digitization from single 2k resolution images. In *Proceedings of the IEEE/CVF Conference on Computer Vision and Pattern Recognition*, pages 12869–12879, 2023. [7](#)
- [7] Shoukang Hu, Fangzhou Hong, Liang Pan, Haiyi Mei, Lei Yang, and Ziwei Liu. Sherf: Generalizable human nerf from a single image. *arXiv preprint arXiv:2303.12791*, 2023. [1](#), [2](#), [3](#), [7](#), [8](#)
- [8] Angjoo Kanazawa, Michael J Black, David W Jacobs, and Jitendra Malik. End-to-end recovery of human shape and pose. In *Proceedings of the IEEE conference on computer vision and pattern recognition*, pages 7122–7131, 2018. [9](#)
- [9] Alex Krizhevsky, Ilya Sutskever, and Geoffrey E Hinton. Imagenet classification with deep convolutional neural networks. *Advances in neural information processing systems*, 25, 2012. [7](#)
- [10] Jason Lawrence, Dan B Goldman, Supreeth Achar, Gregory Major Blascovich, Joseph G Desloge, Tommy Fortes, Eric M Gomez, Sascha Häberling, Hugues Hoppe, Andy Huibers, et al. Project starline: A high-fidelity telepresence system. 2021. [3](#)
- [11] Shanchuan Lin, Linjie Yang, Imran Saleemi, and Soumyadip Sengupta. Robust high-resolution video matting with temporal guidance. In *Proceedings of the IEEE/CVF Winter Conference on Applications of Computer Vision*, pages 238–247, 2022. [9](#)
- [12] Matthew Loper, Naureen Mahmood, Javier Romero, Gerard Pons-Moll, and Michael J Black. Smpl: A skinned multi-person linear model. *Acm Transactions on Graphics*, 34 (Article 248), 2015. [2](#), [3](#), [5](#)
- [13] Ben Mildenhall, Pratul P Srinivasan, Matthew Tancik, Jonathan T Barron, Ravi Ramamoorthi, and Ren Ng. Nerf: Representing scenes as neural radiance fields for view synthesis. *Communications of the ACM*, 65(1):99–106, 2021. [2](#), [3](#)
- [14] Phong Nguyen-Ha, Nikolaos Sarafianos, Christoph Lassner, Janne Heikkilä, and Tony Tung. Free-viewpoint rgb-d human performance capture and rendering. In *European Conference on Computer Vision*, pages 473–491. Springer, 2022. [3](#)
- [15] Sida Peng, Yuanqing Zhang, Yinghao Xu, Qianqian Wang, Qing Shuai, Hujun Bao, and Xiaowei Zhou. Neural body: Implicit neural representations with structured latent codes for novel view synthesis of dynamic humans. In *Proceedings of the IEEE/CVF Conference on Computer Vision and Pattern Recognition*, pages 9054–9063, 2021. [1](#), [2](#), [3](#)
- [16] Shunsuke Saito, Zeng Huang, Ryota Natsume, Shigeo Morishima, Angjoo Kanazawa, and Hao Li. Pifu: Pixel-aligned implicit function for high-resolution clothed human digitization. In *Proceedings of the IEEE/CVF international conference on computer vision*, pages 2304–2314, 2019. [1](#), [2](#), [3](#), [7](#), [8](#)
- [17] Shunsuke Saito, Tomas Simon, Jason Saragih, and Hanbyul Joo. Pifuhd: Multi-level pixel-aligned implicit function for high-resolution 3d human digitization. In *Proceedings of the IEEE/CVF Conference on Computer Vision and Pattern Recognition*, pages 84–93, 2020. [2](#)
- [18] Umme Sara, Morium Akter, and Mohammad Shorif Uddin. Image quality assessment through fsim, ssim, mse and psnr—a comparative study. *Journal of Computer and Communications*, 7(3):8–18, 2019. [7](#)
- [19] Ruizhi Shao, Liliang Chen, Zerong Zheng, Hongwen Zhang, Yuxiang Zhang, Han Huang, Yandong Guo, and Yebin Liu. Floren: Real-time high-quality human performance rendering via appearance flow using sparse rgb cameras. In *SIGGRAPH Asia 2022 Conference Papers*, pages 1–10, 2022. [1](#), [3](#)
- [20] Ruizhi Shao, Hongwen Zhang, He Zhang, Mingjia Chen, Yan-Pei Cao, Tao Yu, and Yebin Liu. Doublefield: Bridging the neural surface and radiance fields for high-fidelity human reconstruction and rendering. In *Proceedings of the IEEE/CVF Conference on Computer Vision and Pattern Recognition*, pages 15872–15882, 2022. [1](#), [2](#), [3](#)
- [21] Gul Varol, Duygu Ceylan, Bryan Russell, Jimei Yang, Ersin Yumer, Ivan Laptev, and Cordelia Schmid. Bodynet: Volumetric inference of 3d human body shapes. In *Proceedings of the European conference on computer vision (ECCV)*, pages 20–36, 2018. [2](#)
- [22] Michael Waechter, Nils Moehrle, and Michael Goesele. Let there be color! large-scale texturing of 3d reconstructions. In *Computer Vision—ECCV 2014: 13th European Conference, Zurich, Switzerland, September 6–12, 2014, Proceedings, Part V 13*, pages 836–850. Springer, 2014. [3](#), [7](#)
- [23] Zhou Wang, Alan C Bovik, Hamid R Sheikh, and Eero P Simoncelli. Image quality assessment: from error visibility to structural similarity. *IEEE transactions on image processing*, 13(4):600–612, 2004. [7](#)
- [24] Yulian Xiu, Jinlong Yang, Xu Cao, Dimitrios Tzionas, and Michael J Black. Econ: Explicit clothed humans obtained from normals. *arXiv preprint arXiv:2212.07422*, 2022. [2](#)
- [25] Yulian Xiu, Jinlong Yang, Dimitrios Tzionas, and Michael J Black. Icon: Implicit clothed humans obtained from normals. In *2022 IEEE/CVF Conference on Computer Vi-*

- sion and Pattern Recognition (CVPR)*, pages 13286–13296. IEEE, 2022. [2](#), [3](#)
- [26] Xueting Yang, Yihao Luo, Yuliang Xiu, Wei Wang, Hao Xu, and Zhaoxin Fan. D-if: Uncertainty-aware human digitization via implicit distribution field. In *Proceedings of the IEEE/CVF International Conference on Computer Vision*, pages 9122–9132, 2023. [3](#)
- [27] Tao Yu, Zerong Zheng, Kaiwen Guo, Pengpeng Liu, Qionghai Dai, and Yebin Liu. Function4d: Real-time human volumetric capture from very sparse consumer rgb-d sensors. In *Proceedings of the IEEE/CVF conference on computer vision and pattern recognition*, pages 5746–5756, 2021. [7](#)
- [28] Richard Zhang, Phillip Isola, Alexei A Efros, Eli Shechtman, and Oliver Wang. The unreasonable effectiveness of deep features as a perceptual metric. In *Proceedings of the IEEE conference on computer vision and pattern recognition*, pages 586–595, 2018. [5](#), [7](#)
- [29] Zerong Zheng, Tao Yu, Yixuan Wei, Qionghai Dai, and Yebin Liu. Deephuman: 3d human reconstruction from a single image. In *Proceedings of the IEEE/CVF International Conference on Computer Vision*, pages 7739–7749, 2019. [2](#)
- [30] Zerong Zheng, Tao Yu, Yebin Liu, and Qionghai Dai. Pamir: Parametric model-conditioned implicit representation for image-based human reconstruction. *IEEE transactions on pattern analysis and machine intelligence*, 44(6): 3170–3184, 2021. [2](#)
- [31] Tiansong Zhou, Jing Huang, Tao Yu, Ruizhi Shao, and Kun Li. Hdhuman: High-quality human novel-view rendering from sparse views. *IEEE Transactions on Visualization and Computer Graphics*, 2023. [1](#), [3](#)